# Canonical form based MAP(2) fitting

**Levente Bodrog**
Technical University of Budapest, Hungary
bodrog@hit.bme.hu

**Peter Buchholz**
Technische Universität Dortmund, Germany
peter.buchholz@cs.uni-dortmund.de

**Jan Kriege**
Technische Universität Dortmund, Germany
jan.kriege@cs.uni-dortmund.de

**Miklós Telek**
Technical University of Budapest, Hungary
telek@hit.bme.hu

Author prepared version of a paper published in Proc. of the 7th International Conference on Quantitative Evaluation of SysTems (QEST 2010), IEEE Computer Society, 2010.

http://doi.ieeecomputersociety.org/10.1109/QEST.2010.22

# Canonical form based MAP(2) fitting

Levente Bodrog
Technical University of Budapest, Hungary
bodrog@hit.bme.hu

Peter Buchholz
Technische Universität Dortmund, Germany
peter.buchholz@cs.uni-dortmund.de

Jan Kriege
Technische Universität Dortmund, Germany
jan.kriege@cs.uni-dortmund.de

Miklós Telek
Technical University of Budapest, Hungary
telek@hit.bme.hu

## Abstract

The importance of the order two Markovian arrival process (MAP(2)) comes from its compactness, serving either as arrival or service process in applications, and from the nice properties which are not available for higher order MAPs. E.g., for order two processes the acyclic MAP(2) (AMAP(2)), the MAP(2) and the order two matrix exponential process (MEP(2)) are equivalent [2]. Additionally, MAP(2) processes can be represented in a canonical form, from which closed form moments bounds are available. In this paper we investigate possible fitting methods utilizing the special nice properties of MAP(2).

We present two fitting methods. One of them partitions the exact boundaries of the MAP(2) class into bounding subsurfaces reducing the numerical inaccuracy of the optimization based moment fitting . The characterizing new feature of the other one is that it considers the distance of joint density functions of infinitely many arrivals.

**Keywords:** MAP(2); arrival process fitting

## 1 Introduction

Markovian arrival processes (MAPs) are widely applied in stochastic modeling. Their popularity comes from their relatively easy applicability and the associated efficient numerical methods (referred to as matrix analytic methods) [11]. MAPs can approximate a wide range of stochastic processes from the simplest renewal processes to the long range dependent, fractal-like and heavy tailed ones [9]. Since it is an important modeling technique researchers pay particular attention to exploring the MAP(n) class but up to now there are still open questions. One of these open questions is, what are the boundaries of the MAP(n) class?

This question is answered only for order two MAPs [2]. The first results on the order two MAPs are given in [5] which presents a basic moment set matching method for hyperexponential MAP(2)s – MAP with hyperexponential marginal distribution. In the next step [6] provides the same results for general acyclic MAPs (AMAPs). Finally [2] proves the equivalence of matrix exponential processes, MAPs and AMAPs of second order as well as [2] provides a minimal Markovian canonical representation of the two dimensional arrival processes.

The knowledge on MAP(2) boundaries can be useful in developing simple models of complex systems as well as in utilizing it as basic building block for large models [4]. Although [2] introduced a moment matching method, together with the derivation of the MAP(2) boundaries, it is not utilized yet for special fitting techniques or to simplify the existing, usually some kind of multidimensional optimization based, fitting algorithms.

In this paper we propose two fitting algorithms utilizing the MAP(2) boundaries and the canonical form. The first method searches for an optimal point in the valid MAP(2) moment space by minimizing the Euclidean distance of the moment sets. The difficulty of this approach comes from the fact that the boundary of the valid MAP(2) moment space is very irregular. Practically the proposed approach is to divide the MAP(2) boundary into "nice" subsurfaces on which the minimization for the distance is constrained. We show that it is worth to do so as the constrained problems can be solved easier than global optimization problems that do not take care of the exact boundaries.

The second fitting algorithm fits MAPs of low order to MAPs of higher order based on the distance of the finite or infinite dimensional joint density functions. In this generally applicable approach we restrict our attention to the case when the low order MAP is MAP(2), because we make use of the MAP(2) canonical form.

We will demonstrate the performance of the proposed algorithms by comparing the cumulative distribution function, the correlation structure and the queueing behavior of the fitted MAP(2)s and the original higher order MAP.

The rest of the paper is organized as follows. First we overview the basic MAP properties in Section 2, then in Section 3 we outline the general approach of MAP fitting by examples of some previously developed methods. The two newly developed fitting algorithms are detailed in Sections 4 and 5. There is a detailed numerical study on the performance of the fitting algorithms given in Section 6. Finally Section 7 concludes the paper.

# 2 Markovian arrival processes

Let $X_0, X_1, \ldots$ be the interarrival times of the arrival process $X(t)$ and let the joint density function of $X_0, X_1, \ldots, X_n$ be defined by the matrix pair $(\mathbf{D}_0, \mathbf{D}_1)$ as

$$\begin{aligned} f(\mathbf{x}) =& f(x_0, x_1, \ldots, x_n) \\ =& \boldsymbol{\pi} e^{\mathbf{D}_0 x_0} \mathbf{D}_1 e^{\mathbf{D}_0 x_1} \mathbf{D}_1 \cdot \cdots \cdot e^{\mathbf{D}_0 x_n} \mathbf{D}_1 \mathbb{1}, \end{aligned} \tag{1}$$

where $\mathbb{1}$ is the column vector of ones and $\boldsymbol{\pi}$ is the solution of the system of linear equations $\boldsymbol{\pi}(-\mathbf{D}_0^{-1})\mathbf{D}_1 = \boldsymbol{\pi}\mathbf{P} = \boldsymbol{\pi}$ and $\boldsymbol{\pi}\mathbb{1} = 1$.

If $\mathbf{D}_0$ is a transient Markovian generator, i.e., $(\mathbf{D}_0)_{ij} \geq 0 \quad \forall i \neq j$, and $(\mathbf{D}_0)_{ii} < 0 \quad \forall i$, $\mathbf{D}_0$ is non-singular and $(\mathbf{D}_1)_{ij} \geq 0 \quad \forall i, j$ such that $-\mathbf{D}_0\mathbb{1} = \mathbf{D}_1\mathbb{1}$ then $f(\mathbf{x})$ is a density function, i.e., $(f(\mathbf{x}) \geq 0) \wedge \left(\int_{\mathbf{x}} f(\mathbf{x}) d\mathbf{x} = 1\right) \quad (\forall n)(\forall \mathbf{x} \geq 0)$, and $X(t)$ is a MAP.

## 2.1 Basic MAP properties

The MAP with representation $(\mathbf{D}_0, \mathbf{D}_1)$ has PH distributed stationary interarrival times with representation $(\boldsymbol{\pi}, \mathbf{D}_0)$, where $\boldsymbol{\pi}$ is the stationary phase distribution after an arrival. Matrix $\mathbf{P} = (-\mathbf{D}_0)^{-1}\mathbf{D}_1$ describes the state transition probabilities of the discrete time Markov chain (DTMC) embedded at the arrival epochs. The probability density function of the PH marginal and its $k$th raw moment are

$$f(t) = \boldsymbol{\pi} e^{\mathbf{D}_0 t} (-\mathbf{D}_0) \mathbb{1} \tag{2}$$

and

$$\mu_k = \mathrm{E}(X^k) = k! \boldsymbol{\pi} (-\mathbf{D}_0)^{-k} \mathbb{1} \tag{3}$$

respectively.

The lag-$k$ correlation of a MAP is

$$\begin{aligned} \mathrm{corr}(X_0, X_k) =& \frac{\mathrm{E}(X_0 X_k) - \mathrm{E}^2(X)}{\mathrm{E}(X^2) - \mathrm{E}^2(X)} \\ =& \frac{\boldsymbol{\pi}(-\mathbf{D}_0)^{-1}\mathbf{P}^k(-\mathbf{D}_0)^{-1}\mathbb{1} - \mu_1^2}{\mu_2 - \mu_1^2}. \end{aligned} \tag{4}$$

A non-redundant MAP(m) (i.e. a MAP for which no equivalent MAP(o) with $o < m$ exists) is determined by the so-called basic moment set, containing $m^2$ reduced (joint) moments [3]. In case of MAP(2) a process is defined by four parameters. They are the first 3 moments defining the PH(2) marginal distribution and the lag-1 correlation defining the, geometrically decaying, correlation structure of the process.

## 2.2 The moment boundaries of the MAP(2) set

Instead of working with the first 3 moments and the lag-1 correlation it is often beneficial to work with dimensionless quantities. In MAP(2) analysis the use of normalized moments [13] and the correlation coefficient became popular. The normalized moments are defined as

$$n_k = \frac{\mu_k}{\mu_{k-1}\mu_1}, \quad k \geq 2, \tag{5}$$

whilst [7] defines the shape parameter $\gamma$ of the geometric decaying autocorrelation function of the MAP(2) class as

$$\mathrm{corr}(X_0, X_k) = \frac{\mathrm{E}(X_0 X_k) - \mu_1^2}{\mu_2 - \mu_1^2} = \gamma^k \frac{\frac{n_2}{2} - 1}{n_2 - 1}. \tag{6}$$

As a result of (5) and (6) we can represent a MAP(2) with $\mu_1$ (multiple of the time unit) and 3 dimensionless quantities $n_2, n_3, \gamma$. In case of parameter matching $\mu_1$ is easy to match independently of the other parameters since for a positive constant $c$ with $\mathbf{D}_0' = c\mathbf{D}_0$, and $\mathbf{D}_1' = c\mathbf{D}_1$ we have

$$\begin{aligned} \mu_1' &= \mu_1/c, \\ n_k' = \frac{\mu_k'}{\mu_{k-1}'\mu_1'} &= \frac{c^{-k}\mu_k}{c^{-(k-1)}\mu_{k-1}c^{-1}\mu_1} = \frac{\mu_k}{\mu_{k-1}\mu_1} = n_k, \\ \mathrm{E}(X_0' X_k') &= \boldsymbol{\pi}(-c\mathbf{D}_0)^{-1}\mathbf{P}^k(-c\mathbf{D}_0)^{-1}\mathbb{1} = c^{-2}\,\mathrm{E}(X_0 X_k), \\ \mathbf{P}' &= (-c\mathbf{D}_0)^{-1}(c\mathbf{D}_1) = (-\mathbf{D}_0)^{-1}\mathbf{D}_1 = \mathbf{P} \end{aligned}$$

and

$$\gamma' = \frac{\mathrm{E}(X_0' X_1') - {\mu_1'}^2}{\frac{\mu_2'}{2} - {\mu_1'}^2} = \frac{c^{-2}\,\mathrm{E}(X_0 X_1) - (c^{-1}\mu_1)^2}{\frac{c^{-2}\mu_2}{2} - (c^{-1}\mu_1)^2} = \gamma.$$

Hence, our focus is on the matching/fitting of the dimensionless quantities $n_2, n_3, \gamma$.

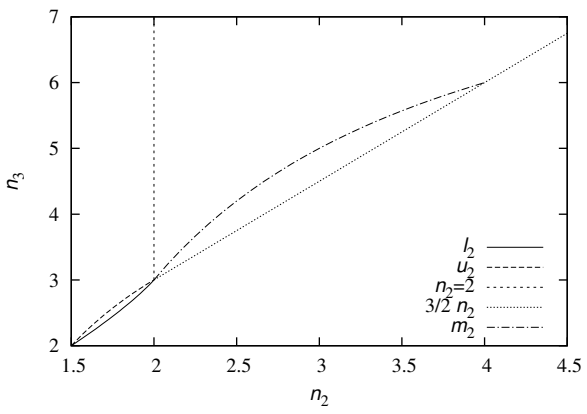


Figure 1: The PH(2) boundaries on the $(n_2, n_3)$ plane

**The boundaries of the PH(2) marginal distribution [1]** The marginals of a MAP(2) are PH(2) distributed and are characterized by $\mu_1$ and $(n_2, n_3)$. The bounds for $(n_2, n_3)$ are as follows [1].

$$\frac{3}{2} \leq n_2. \tag{7}$$

To give the bounds of the third normalized moment first we introduce simplifying notations

$$p_2 = \frac{3(n_2-2)}{3n_2}\left(\frac{-2\sqrt{3}}{\sqrt{12-6n_2}} - 1\right),$$
$$a_2 = \frac{n_2-2}{p_2(1-n_2)+\sqrt{p_2^2+(2p_2(n_2-2))}},$$
$$l_2 = \frac{3(a_2+1)}{a_2p_2+1} - \frac{6a_2}{2+a_2p_2(2a_2+2)}, \tag{8}$$
$$u_2 = \frac{6(n_2-1)}{n_2}. \tag{9}$$

Using these notations we can express the third normalized moment bounds by its lower

$$l_2 \leq n_3, \quad \text{if } \frac{3}{2} \leq n_2 \leq 2 \tag{10a}$$
$$\frac{3}{2}n_2 < n_3, \quad \text{if } 2 \leq n_2 \tag{10b}$$

and upper bounds

$$n_3 \leq u_2, \quad \text{if } \frac{3}{2} \leq n_2 \leq 2 \tag{10c}$$
$$n_3 < \infty, \quad \text{if } 2 < n_2. \tag{10d}$$

The boundaries of the PH(2) class, together with the curve (13), are summarized in Figure 1.

The boundaries of the $\gamma$ parameter are provided in [2] and are summarized in Table 1.

### 2.3 MAP(2) canonical form

The canonical form (CF) of the MAP(2) class has two variants depending on the sign of the correlation parameter [2]. In both variants the canonical form is given in terms of the rate parameters $0 < \lambda_1 \leq \lambda_2$ and probabilities $0 \leq a \leq 1$ and $0 \leq b \leq 1$.

**The canonical form when $\gamma \geq 0$, CF 1** For a MAP(2) with positive $\gamma$ the canonical matrix representation has the form

$$\mathbf{D}_0 = \begin{pmatrix} -\lambda_1 & (1-a)\lambda_1 \\ 0 & -\lambda_2 \end{pmatrix}, \quad \mathbf{D}_1 = \begin{pmatrix} a\lambda_1 & 0 \\ (1-b)\lambda_2 & b\lambda_2 \end{pmatrix}. \tag{11}$$

Additional requirements on the parameters are $a, b \neq 1$ for recurrency. The stationary phase distribution after an arrival for CF 1 is $\boldsymbol{\pi} = \left(\frac{1-b}{1-ab} \;\; \frac{b-ab}{1-ab}\right)$.

**The canonical form when $\gamma < 0$, CF 2** For negative $\gamma$ MAP(2) has the canonical form

$$\mathbf{D}_0 = \begin{pmatrix} -\lambda_1 & (1-a)\lambda_1 \\ 0 & -\lambda_2 \end{pmatrix}, \quad \mathbf{D}_1 = \begin{pmatrix} 0 & a\lambda_1 \\ b\lambda_2 & (1-b)\lambda_2 \end{pmatrix}. \tag{12}$$

Additional requirements on the parameters are $b \neq 0$ for recurrency and $\lambda_1 \neq \lambda_2$ if $a = 1$ for a valid order two process. The stationary phase distribution after an arrival for CF 2 is $\boldsymbol{\pi} = \left(\frac{b}{1+ab} \;\; 1-\frac{b}{1+ab}\right)$.

## 3 Approximate fitting algorithms

The availability of explicit expressions that define the parameters of the canonical MAP(2) form based on the moment set $(\mu_1, n_2, n_3, \gamma)$ makes moments matching an obvious job when the moments to be fitted are within the MAP(2) moment bounds (Section 2.2). Unfortunately, to find the best MAP(2) approximate of a moment set which is outside the valid MAP(2) moment boundaries is a far more complex task.

This section compares some general purpose optimization algorithms for solving this problem. The general fitting approach is to optimize some distance measure over the MAP(2) class.

There are various options for defining a distance of the moment sets. We made several comparisons and found that with respect to the properties we are interested in (the benefit of optimizing with Algorithm 2) all reasonable distances behave similarly. Throughout

Table 1: The MAP(2) $\gamma$ bounds in terms of the normalized moments

| condition | $\gamma$ bound | |
|---|---|---|
| | lower | upper |
| $n_2 < 2$ | $-\frac{n_2(n_3-6)+6}{3n_2-6}$ | $-\frac{2\left(\frac{1}{2}(n_2-2)+\frac{1}{2}\sqrt{n_2^2-\frac{2n_2n_3}{3}}\right)^2}{n_2-2}$ |
| $n_2 > 2 \wedge n_3 < 9-\frac{12}{n_2}$ | $-\frac{n_2(n_3-6)+6}{3n_2-6}$ | 1 |
| $n_2 > 2 \wedge 9-\frac{12}{n_2} \geq n_3$ | $\frac{n_2(n_3-9)-\sqrt{n_2\left(n_2\left(18n_2+n_3(n_3-18)-27\right)+24n_3\right)+12}}{n_2(n_3-9)+\sqrt{n_2\left(n_2\left(18n_2+n_3(n_3-18)-27\right)+24n_3\right)+12}}$ | 1 |

the paper we use the Euclidean distance, or simply distance, of the basic moment sets

$$\mathrm{d}\big((\mu_1,n_2,n_3,\gamma),(\mu_1',n_2',n_3',\gamma')\big) = \sqrt{(\mu_1-\mu_1')^2+(n_2-n_2')^2+(n_3-n_3')^2+(\gamma-\gamma')^2}.$$

As there is no widely applied measure for fitting and since the Euclidean distance is the most natural distance over the three dimensional space, we use this distance measure to show how the decomposition of the MAP(2) bounds can improve the moment fitting. The same concept can be applied for any other distance measure to which the moment bounds, given in Table 1, can be transformed, e.g., weighted moment distance. We do not search for the "the best" distance measure in the paper.

## 3.1 Global optimization

Having the boundaries of the MAP(2) class in the moment space and a non MAP(2) point (a point outside the valid MAP(2) moment set) it seems obvious to define a distance and minimize it subject to the MAP(2) set. In case of a convex surface it is numerically stable but in case of the MAP(2) class there are two tangential parts of the subset over the $(n_2, n_3)$ plane and also the $\gamma$ boundaries are built up of five separate surfaces.

The problem is that the accuracy of such a fitting method highly depends on the performance of the applied optimization algorithm, especially in case of a concave and not differentiable surface. How does the distance "change" between the tangential subspaces especially as the MAP(2) class does not contain the point of tangency? How can the method "leave" local minima to find the global one? In which way does it depend on its initial settings? etc...

In the following example we used several, numerical, nonlinear optimization methods to find the closest fitting MAP(2) to an external point based on the Euclidean distance. The investigated optimization methods are

- Nelder-Mead [12],
- differential evolution [14],
- simulated annealing [16], [10] and
- random search.

All of them have several settings and each of them needs special attention that we left for the automatic setup mechanism of Mathematica.

To demonstrate the performance of the investigated optimization methods we simply take a point on the $(n_2, n_3, 0)$ plane, namely $(1, 22, 0)$, to fit to. The results are given in the first 4 rows of Table 3.1 for each of the algorithms.

Table 2: Result of fitting on $(1, 22, 0)$ by several moment fitting algorithms

| method | distance | result $(n_2, n_3, \gamma)$ |
|---|---|---|
| Nelder-Mead | 19.0378 | $(2.005, 3.015, 0.9993)$ |
| differential evolution | 18.8955 | $(2.0918, 3.1379, 0.2645)$ |
| simulated annealing | 19.8389 | $(1.5756, 2.1694, 0.00069)$ |
| random search | 19.3223 | $(1.8448, 2.6963, 0.0431)$ |
| OMAM | $\frac{\sqrt{1601}}{2} \simeq 20$ | $(\frac{3}{2}, 2, 0)$ |
| decomp. numerical fitting | 1 | $(2, 22, 0)$ |

According to our experiences the results in Table 3.1 are typical. The performance of the general purpose optimization methods are similarly poor. In the rest of the paper we report only the results of the Nelder-Mead method among the general purpose optimization methods, but the other (differential evolution, simulated annealing and random search) exhibit similar properties.

### 3.2 Ordered Moment Adjusting Method (OMAM)

If one knows the exact boundaries of the MAP(2) class and looks for a MAP(2) fitting of a non MAP(2) moment set $(n_2, n_3, \gamma)$ there are several possibilities. Setting the moments out of the valid range separately gives the best approximation moment by moment. At the first sight it seems that this is enough, but doing so completely ignores the "perpendicular directions of a gradient defined as a measure in the moment space". This latter behavior results in a suboptimal solution of an optimization problem trying to minimize the given measure over the moment space in several steps. The problem of this policy is that the result depends on the order of the adjustment. We show this through an example using Algorithm 1 describing OMAM.

**Algorithm 1** `ordered moment adjusting method`

**INPUT:** $\mathbf{v} = (n_2, n_3, \gamma)$
**OUTPUT:** $(\mathbf{D}_0, \mathbf{D}_1)$
1: **for** $i = 0$ to $2$ **do**
2: **if** $(\mathbf{v})_i$ falls out of the feasible range of that "moment" **then**
3: adjust it to be on the closer bound given either in [15] or in [2]
4: **else**
5: leave $(\mathbf{v})_i$ unchanged
6: $(\mathbf{D}_0, \mathbf{D}_1) \leftarrow \mathbf{v}$
7: **return** $(\mathbf{D}_0, \mathbf{D}_1)$

Having the outer, non MAP(2), point $M = (8, 9, 0)$ the resulting moment set of the fitting after the loop, through lines 1 and 5 in Algorithm 1, is $\hat{M}_1 = (6, 9, 0)$. While if the adjustment of $n_3$ precedes that of $n_2$ then the resulting MAP will have the coordinates $\hat{M}_2 = (8, 12, 0)$. This small example shows the importance of the fitting order of the moments.

The distance of $\hat{M}_1$ from the outer point $(M)$ is $d_1 = \mathrm{d}\left(\hat{M}_1, M\right) = 2$ and the distance of $\hat{M}_2$ is $d_2 = \mathrm{d}\left(\hat{M}_2, M\right) = 3$. Although $d_1 < d_2$ none of them gives the aimed closest MAP point since the distance of $\hat{M} = \left(\frac{86}{13}, \frac{129}{13}, 0\right)$ is $d = \mathrm{d}\left(\hat{M}, M\right) = \frac{6}{\sqrt{13}} < 2$. Here we note that the above approximate points are on the open border of the MAP(2), i.e., they are not MAP(2)s themselves, but they demonstrate clearly the problem with OMAM.

A possible usage of Algorithm 1 is the case when the fitting of different moments has different priorities. Moments with lower priority are then adjusted later.

## 4 Decomposed numerical fitting method

Since the problem of global optimization based method results from the fact that the MAP(2) bounding surface is concave and not differentiable, we try to utilize the knowledge about the MAP(2) boundaries (see Section 2.2).

Technically the MAP(2) boundaries are built up of ten parts. Here we give the formal description of them as well as the decomposed numerical fitting method based on the partitioning.

### 4.1 Division of the MAP(2) bounding surface

The bounding surface of the MAP(2) moments set can be divided into parts with nice surface properties. Indeed the definition of the surface in Table 1 already suggests the evident way of dividing the surfaces into parts. This division is presented in Table 2 where the parts are numbered from I to X.

Additionally we define the curve

$$m_2 = 9 - \frac{12}{n_2}. \tag{13}$$

Subsurfaces III, VIII, IX and X are vertical surfaces in the $(n_2, n_3, \gamma)$ space. In particular

- subsurface III is the vertical bound between subsurfaces I and II,
- subsurface VIII is the vertical bound between subsurfaces V and VII, along $n_2 = 2$,
- subsurface IX is the vertical bound between subsurfaces IV and VII and
- subsurface X is the vertical bound between subsurfaces V and VII, along $n_3 = \frac{3}{2}n_2$ for $n_2 \geq 4$

applying the appropriate constraints on all coordinates.

Figure 2(a) summarizes all the nonvertical surfaces appearing in Table 2, whilst Figure 2(b) enlarges the same for subsurfaces I and II. In Figure 2(a) there are also the lower bounding $\gamma$ surfaces (subsurfaces I, IV, V and VI) mapped onto the base plane on which the same division of the $(n_2, n_3)$ plane appears as in Figure 1.

### 4.2 The decomposed numerical fitting method

Based on the poor performance of the general purpose optimization methods and the structure of the

Table 3: The MAP(2) bounding subsurfaces

| the surface given by its coordinates | ID | condition(s) |
|---|---|---|
| $\left(n_2, n_3, -\frac{n_2(n_3-6)+6}{3n_2-6}\right)$ | I | $\frac{3}{2} \le n_2 < 2, \quad l_2 \le n_3 \le u_2$ |
| $\left(n_2, n_3, -\frac{\frac{1}{2}\left(n_2+\sqrt{n_2^2-\frac{2n_2n_3}{3}}-2\right)^2}{n_2-2}\right)$ | II | $\frac{3}{2} \le n_2 < 2, \quad l_2 \le n_3 \le u_2$ |
| $(n_2, l_2, \gamma)$ | III | $\frac{3}{2} \le n_2 < 2, \quad -\frac{n_2(l_2-6)+6}{3n_2-6} < \gamma < -\frac{\frac{1}{2}\left(n_2+\sqrt{n_2^2-\frac{2n_2l_2}{3}}-2\right)^2}{n_2-2}$ |
| $\left(n_2, n_3, -\frac{n_2(n_3-6)+6}{3n_2-6}\right)$ | IV | $2 < n_2 < 4, \quad \frac{3}{2}n_2 < n_3 < m_2$ |
| $\left(n_2, n_3, \frac{n_2(n_3-9)-\sqrt{n_2\left(n_2\left(18n_2+n_3(n_3-18)-27\right)+24n_3\right)+12}}{n_2(n_3-9)+\sqrt{n_2\left(n_2\left(18n_2+n_3(n_3-18)-27\right)+24n_3\right)+12}}\right)$ | V | $2 < n_2 < 4, \quad m_2 \le n_3$ |
| $\left(n_2, n_3, \frac{n_2(n_3-9)-\sqrt{n_2\left(n_2\left(18n_2+n_3(n_3-18)-27\right)+24n_3\right)+12}}{n_2(n_3-9)+\sqrt{n_2\left(n_2\left(18n_2+n_3(n_3-18)-27\right)+24n_3\right)+12}}\right)$ | VI | $4 \le n_2, \quad \frac{3}{2}n_2 < n_3$ |
| $(n_2, n_3, 1)$ | VII | $2 < n_2, \quad \frac{3}{2}n_2 < n_3$ |
| $(2, n_3, \gamma)$ | VIII | $3 < n_3, \quad \frac{n_3-\sqrt{(n_3-3)^2}-3}{n_3+\sqrt{(n_3-3)^2}-3} < \gamma < 1$ |
| $\left(n_2, \frac{3}{2}n_2, \gamma\right)$ | IX | $2 < n_2 < 4, \quad 1-\frac{n_2}{2} < \gamma < 1$ |
| $\left(n_2, \frac{3}{2}n_2, \gamma\right)$ | X | $4 \le n_2, \quad \frac{n_2(n_2-6)-\sqrt{n_2^2(n_2-2)^2+8}}{n_2(n_2-6)+\sqrt{n_2^2(n_2-2)^2+8}} < \gamma < 1$ |

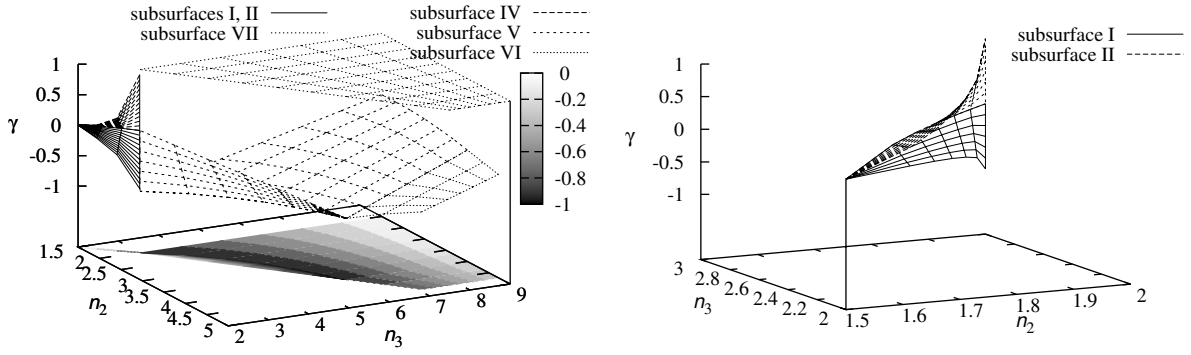


(a) All the nonvertical subsurfaces

(b) The nonvertical subsurfaces for $\frac{3}{2} \le n_2 < 2$

Figure 2: The moment bounds of the set of MAP(2) distribution in the $(n_2, n_3, \gamma)$ space

MAP(2) moments bounding surface it seems reasonable to decompose the problem into optimization over nice surfaces and take the best of the obtained solutions. We name this approach decomposed numerical fitting method.

Similar to the global optimization based fitting methods in Section 3.1 our fitting algorithm also tries to minimize the Euclidean distance between the given outer point and the MAP(2) subspace. The difference is that here we use the decomposition of the bounding surface and the associated constraints, i.e., the computational complexity of the method is the same as the global optimization based but the probability of finding the global optimum is enlarged.

Our method utilizes that the Euclidean distance between an outer point and a region lies on the border of that region. Accordingly it goes through the bounding subsurfaces, given in Table 2, finds the minima of the distance between the actual subsurface and the outer point and return with the closest point and its distance from the outer point. This is expressed briefly in Algorithm 2.

**Algorithm 2** `decomposed numerical fitting method`

**INPUT:** $M = (n_2, n_3, \gamma)$ the outer point
**OUTPUT:** $(\mathbf{D}_0, \mathbf{D}_1, d)$ the closest MAP(2) and its distance from $M$

1: $d = \infty$
2: **while** there is unchecked subsurface **do**
3: find the closest point $(\tilde{M})$ on the actual surface from $M$
4: calculate the Euclidean distance of $\tilde{M}$ and $M$ $\tilde{d} = d(M, \tilde{M})$
5: **if** $\tilde{d} < d$ **then**
6: $d = \tilde{d}$
7: $\hat{M} = \tilde{M}$
8: consider the "next" subsurface
9: $(\mathbf{D}_0, \mathbf{D}_1) \leftarrow \hat{M}$
10: **return** $(\mathbf{D}_0, \mathbf{D}_1, d)$

# 5 Fitting high order MAPs with low order MAPs

There are several modeling situations when the size of the MAP models needs to be reduced for efficient numerical computations. E.g., there are fitting methods which generate large MAPs that allow an easy setting of the required parameters [4]; in queuing network analysis the size of the traffic descriptors might increase during the course of the analysis, etc. In these situations it is necessary to reduce the size of the MAP eventually.

A possible way for this reduction is to match a smaller MAP to the low order moments of the large MAP [8]. It is an efficient approach as long as the low order moments of the large MAP are inside the moments bounds of the small one. But when it is not the case the problems discussed in the previous sections arise.

In this section we present an alternative approach for fitting large MAPs with smaller ones. To utilize the known bounds of the MAP(2) class we assume that the small MAP is MAP(2), but the approach is applicable for larger MAPs as well.

Due to the fact that the stochastic process we would like to approximate is a MAP, whose analytical properties are known, we can go beyond minimizing moments based distance measures. We can define distances between joint densities of finite and also for infinite number of inter-arrivals.

Equation (1) gives the joint density of the interarrival times of a MAP $X(t)$. Having two MAPs of order $m$ and $o$, with joint densities $f(\cdot)$ and $g(\cdot)$, and representations $(\mathbf{D}_0, \mathbf{D}_1)$ and $(\mathbf{G}_0, \mathbf{G}_1)$, and stationary phase distributions $\boldsymbol{\pi}$ and $\boldsymbol{\gamma}$, respectively, the integral of the product of their joint densities can be expressed as

$$
\begin{aligned}
L_{fg}(n) &= \int_{\mathbf{x}} f(x_1, x_2, \cdots, x_n) g(x_1, x_2, \cdots, x_n) d\mathbf{x} \\
&= \int_{\mathbf{x}} \left(\boldsymbol{\pi} e^{\mathbf{D}_0 x_1} \mathbf{D}_1 e^{\mathbf{D}_0 x_2} \mathbf{D}_1 \cdots e^{\mathbf{D}_0 x_n} \mathbf{D}_1 \mathbb{1}\right) \\
&\quad \otimes \left(\boldsymbol{\gamma} e^{\mathbf{G}_0 x_1} \mathbf{G}_1 e^{\mathbf{G}_0 x_2} \mathbf{G}_1 \cdots e^{\mathbf{G}_0 x_n} \mathbf{G}_1 \mathbb{1}\right) d\mathbf{x} \\
&= \int_{\mathbf{x}} (\boldsymbol{\pi} \otimes \boldsymbol{\gamma}) \left(e^{\mathbf{D}_0 x_1} \otimes e^{\mathbf{G}_0 x_1}\right) (\mathbf{D}_1 \otimes \mathbf{G}_1) \times \ldots \\
&\quad \times \left(e^{\mathbf{D}_0 x_n} \otimes e^{\mathbf{G}_0 x_n}\right) (\mathbf{D}_1 \otimes \mathbf{G}_1) (\mathbb{1} \otimes \mathbb{1}) d\mathbf{x} \\
&= (\boldsymbol{\pi} \otimes \boldsymbol{\gamma}) \left(\int_{x_1} e^{\mathbf{D}_0 x_1} \otimes e^{\mathbf{G}_0 x_1} dx_1\right) (\mathbf{D}_1 \otimes \mathbf{G}_1) \times \ldots \\
&\quad \times \left(\int_{x_n} e^{\mathbf{D}_0 x_n} \otimes e^{\mathbf{G}_0 x_n} dx_n\right) (\mathbf{D}_1 \otimes \mathbf{G}_1) (\mathbb{1} \otimes \mathbb{1}) \\
&= \underbrace{(\boldsymbol{\pi} \otimes \boldsymbol{\gamma})}_{\boldsymbol{\nu}} \underbrace{\left(-\left(\mathbf{D}_0 \oplus \mathbf{G}_0\right)^{-1} (\mathbf{D}_1 \otimes \mathbf{G}_1)\right)^n}_{\mathbf{N}^n} \underbrace{(\mathbb{1} \otimes \mathbb{1})}_{\mathbb{1}} \\
&= \boldsymbol{\nu} \mathbf{N}^n \mathbb{1}.
\end{aligned}
\tag{14}
$$

Here $n$ is the number of considered interarrivals, i.e., the number of the considered samples in the two arrival processes.

### 5.1 Computing distances between MAPs based on $L(n)$

The compact, and easy to compute form of (14) can be utilized also in evaluating the distances of MAPs. Assume that there is a given MAP with representation $(\mathbf{D}_0, \mathbf{D}_1)$ and we are looking for a smaller MAP with representation $(\mathbf{G}_0, \mathbf{G}_1)$. In this case, the optimization problem of the distance of the joint density functions of the two MAPs is

$$\begin{aligned}
&\min_{\mathbf{G}_0,\mathbf{G}_1} d\big(f(\mathbf{x}), g(\mathbf{x})\big) = \\
&= \min_{\mathbf{G}_0,\mathbf{G}_1} \int_{\mathbf{x}} \big(f(\mathbf{x}) - g(\mathbf{x})\big)^2 d\mathbf{x} \\
&= \min_{\mathbf{G}_0,\mathbf{G}_1} \Bigg( \int_{\mathbf{x}} f(\mathbf{x}) f(\mathbf{x}) d\mathbf{x} + \int_{\mathbf{x}} g(\mathbf{x}) g(\mathbf{x}) d\mathbf{x} \\
&\quad -2 \int_{\mathbf{x}} f(\mathbf{x}) g(\mathbf{x}) d\mathbf{x} \Bigg) \\
&= \min_{\mathbf{G}_0,\mathbf{G}_1} \Big( L_{ff}(n) + L_{gg}(n) - 2L_{fg}(n) \Big).
\end{aligned} \tag{15}$$

Using (14) for the three terms on the right hand side of (15) the function that has to be minimized can be easily computed.

Furthermore, knowing the general canonical form of the second order MAPs, as given in (11) and (12), with four variables $(a, b, \lambda_1, \lambda_2)$ the optimization in (15) reduces to a four dimensional minimization problem.

### 5.2 Reducing the MAP order according to the dominant Eigenvalue of N

Based on the spectral decomposition of $\mathbf{N}$ equation (14) can be rewritten as

$$L_{fg}(n) = \boldsymbol{\nu} \mathbf{N}^n \mathbb{1} = \sum_{i=1}^{s} \sum_{j=0}^{\alpha_i} a_{ij} \lambda_i^{n-j}, \tag{16}$$

where $\lambda_i$ are the roots, with multiplicity $\alpha_i$, of the minimal polynomial of $\mathbf{N}$ and $a_{ij}$ are the appropriate constants. If the size of the fitted and the original MAPs are $m$ and $o$ then $s \leq mo$. Taking the limit of (16) as $n$ tends to $\infty$ we have that

$$\lim_{n\to\infty} L_{fg}(n) = \lim_{n\to\infty} \boldsymbol{\nu} \mathbf{N}^n \mathbb{1} = \lim_{n\to\infty} \sum_{i=1}^{s} \sum_{j=0}^{\alpha_i - 1} a_{ij} \lambda_i^{n-j} = c \lambda_d^n \tag{17}$$

where $c = \sum_{j=0}^{\alpha_d - 1} a_{dj} \lambda_d^{-j}$ is constant and $\lambda_d$ is the dominant eigenvalue of matrix $\mathbf{N}$, i.e., $L_{fg}(n) \sim \lambda_d^n$ as $n \to \infty$. Here we assumed that $\lambda_d$ is real, which fits with our experiences.

While in the previous section we assumed a fixed $n$ for the exponent of (14) here we assume that $n \to \infty$.

Let $\lambda_f$, $\lambda_g$ and $\lambda_{fg}$ be the dominant eigenvalues corresponding to the terms $L_{ff}(n)$, $L_{gg}(n)$ and $L_{fg}(n)$ respectively. Using (17) the optimization problem simplifies to

$$\min_{\mathbf{G}_0,\mathbf{G}_1} \left(\lambda_f + \lambda_g - 2\lambda_{fg}\right). \tag{18}$$

## 6 Numerical study

Our experiments can be divided into two parts. In the first part we investigate the performance of our methods by fitting a MAP(2) on a random five dimensional MAP with moments falling outside the MAP(2) moments region. In the second part we apply moment matching on a random three dimensional MAP with moments within the MAP(2) moments region. In the second part we apply the MAP reduction approach of Section 5 and also verify the moment matching method. In both cases we compare the cumulative distribution function, the correlation structure and the queueing behavior of the resulting MAP(2) with the original MAP.

The methods can be applied to any experimental data without any restrictions. In case of decomposed fitting the goodness of fit is determined by the used distance measure (here it is the Euclidean distance) while in case of the MAP reduction technique one should first fit an arbitrary large MAP to the trace and then the reduction can be applied. For our purposes, to show the efficiency of the algorithms, it is sufficient to evaluate the approach with random MAPs.

### 6.1 Fitting a MAP(5)

We apply the proposed methods for fitting a MAP(2) to the random, five dimensional, MAP with matrix representation

$$\begin{aligned}
\mathbf{D}_0 &= \begin{pmatrix} -3 & 1 & 0 & 0 & 0 \\ 1 & -5 & 0 & 0 & 0 \\ 0 & 1 & -4 & 0 & 0 \\ 1 & 0 & 0 & -2 & 0 \\ 1 & 0 & 0 & 1 & -5 \end{pmatrix}, \\
\mathbf{D}_1 &= \begin{pmatrix} 1 & 0 & 0 & 1 & 0 \\ 0 & 1 & 1 & 1 & 1 \\ 1 & 0 & 1 & 0 & 1 \\ 0 & 0 & 0 & 1 & 0 \\ 0 & 1 & 1 & 1 & 0 \end{pmatrix}.
\end{aligned} \tag{19}$$

The moments of this MAP(5) are $(n_2 = 1.96161, n_3 = 2.88108, \gamma = -0.237176)$. This point is outside the MAP(2) moment region. Its first raw moment is $\mu_1 = 0.560976$.

Once we have $(n_2 = 1.96161, n_3 = 2.88108, \gamma = -0.237176)$ we fit MAP(2) to it using

- the global optimization with the Nelder-Mead method, as described in Section 3.1,
- OMAM, as described in Section 3.2,
- the decomposed fitting method, as given in Section 4, to fit
  - directly the shape parameter ($\gamma$), or equivalently the lag-1 correlation coefficient $\rho_1 = \gamma\frac{\frac{n_2}{2}-1}{n_2-1}$,
  - the lag-9 correlation coefficient $\rho_9 = \gamma^9\frac{\frac{n_2}{2}-1}{n_2-1}$ and
  - a higher lag, $\rho_{99} = \gamma^{99}\frac{\frac{n_2}{2}-1}{n_2-1}$, both of them used to express the shape parameter as $\gamma = \sqrt[n]{\rho_n\frac{n_2-1}{\frac{n_2}{2}-1}}$ and
  - the dominant eigenvalue ($\lambda_d$) of the DTMC embedded at arrival epochs.
- The joint density function fitting for the exponent $n = 10$, as given in Section 5.1, and
- the dominant eigenvalue based joint density function fitting, as presented in Section 5.2.

The resulting moment triples are summarized in Table 3. We note that the MAP reduction procedure results in different first raw moment while in the moment based fittings method we can set the original one, $\mu_1 = 0.560976$.

It can be seen in Table 3 that all the fitting methods give quite close results in terms of the Euclidean distance. And as we expected the decomposed moment fitting (eg) and OMAM (ma) give significant good results.

For further investigations we first determine the corresponding matrix representations for all the fitted MAP(2)s using the four element basic moment set $(\mu_1, n_2, n_3, \gamma)$.

$$\mathbf{D}_0^{(\mathrm{nm})} = \begin{pmatrix} -1.698 & 0.0006 \\ 0 & -1.877 \end{pmatrix} \qquad \mathbf{D}_1^{(\mathrm{nm})} = \begin{pmatrix} 0 & 1.698 \\ 1.876 & 0.0006 \end{pmatrix} \tag{20}$$

$$\mathbf{D}_0^{(\mathrm{ma})} = \begin{pmatrix} -2.069 & 0.944 \\ 0 & -2.069 \end{pmatrix} \qquad \mathbf{D}_1^{(\mathrm{ma})} = \begin{pmatrix} 0 & 1.125 \\ 0.903 & 1.167 \end{pmatrix} \tag{21}$$

$$\mathbf{D}_0^{(\mathrm{eg})} = \begin{pmatrix} -2.093 & 1.002 \\ 0 & -2.098 \end{pmatrix} \qquad \mathbf{D}_1^{(\mathrm{eg})} = \begin{pmatrix} 0 & 1.091 \\ 0.955 & 1.143 \end{pmatrix} \tag{22}$$

$$\mathbf{D}_0^{(\mathrm{r9})} = \begin{pmatrix} -1.763 & 6.553\times10^{-5} \\ 0 & -1.802 \end{pmatrix} \qquad \mathbf{D}_1^{(\mathrm{r9})} = \begin{pmatrix} 0 & 1.7633 \\ 1.802 & 0 \end{pmatrix} \tag{23}$$

$$\mathbf{D}_0^{(\mathrm{r99})} = \begin{pmatrix} -1.787 & 0.008 \\ 0 & -1.787 \end{pmatrix} \qquad \mathbf{D}_1^{(\mathrm{r99})} = \begin{pmatrix} 0 & 1.779 \\ 1.787 & 0 \end{pmatrix} \tag{24}$$

$$\mathbf{D}_0^{(\mathrm{ed})} = \begin{pmatrix} -2.095 & 0.714 \\ 0 & -2.096 \end{pmatrix} \qquad \mathbf{D}_1^{(\mathrm{ed})} = \begin{pmatrix} 1.382 & 0 \\ 0.557 & 1.538 \end{pmatrix} \tag{25}$$

$$\mathbf{D}_0^{(\mathrm{lh})} = \begin{pmatrix} -1.733 & 0.121 \\ 0 & -5.939 \end{pmatrix} \qquad \mathbf{D}_1^{(\mathrm{lh})} = \begin{pmatrix} 1.612 & 0 \\ 3.317 & 2.622 \end{pmatrix} \tag{26}$$

$$\mathbf{D}_0^{(\mathrm{ld})} = \begin{pmatrix} -1.7137 & 0.162 \\ 0 & -4.7576 \end{pmatrix} \qquad \mathbf{D}_1^{(\mathrm{ld})} = \begin{pmatrix} 1.551 & 0 \\ 2.367 & 2.391 \end{pmatrix} \tag{27}$$

Once we have the matrix representation we can calculate the fitted parameters. In case of methods (r9), (r99) these are $\rho_9^{(r9)} = -0.000120081$ and $\rho_{99}^{(r99)} = 3.20821 \times 10^{-6}$, respectively, while the original MAP(5) has the parameter values $\rho_9 = 0.0000320486$ and $\rho_{99} = 1.41312 \times 10^{-33}$. The bad match of the correlation parameters are caused by their very low values and accordingly the limited numerical accuracy which attracts our attention to the numerical stability of the decomposed fitting method for low values although it seems more accurate than the global optimizations in the same space.

In case of the fitting method (ed) the dominant eigenvalue of the DTMC embedded at arrival epochs is fitted. For the original MAP(5) it is $\lambda_d = 0.484103$ and for the fitted MAP(2) it is $\gamma = 0.484102$ which is a very good match.

**PH(2) fitting** The cumulative distribution function (CDF) of the PH marginal distributions for the original MAP(5) and for all the fitted MAP(2)s are calculated using their matrix representations in (19) and in (20) through (27) and their stationary phase distributions as

$$F(x) = 1 - \boldsymbol{\pi} e^{\mathbf{D}_0 x} \mathbb{1}, \tag{28}$$

where $\boldsymbol{\pi}$ is the stationary phase distribution after an arrival and $\mathbf{D}_0$ is the transient generator of the PH marginal of the MAP. The resulting MAP(2)s fit the MAP(5) reasonably well, the CDFs show a good match with the original one in Figure 3(a). Figure 3(b) shows that (nm) fits best the body and (eg), (ed), (lh) and (ld) the tail of the distribution.

**Lag-$k$ fitting** The correlation structure of all the original and the fitted MAPs are calculated by the consecutive evaluation of (4) and is depicted in Figure 3(c). Those methods which find a correlation parameter close to 1 result in a very slow correlation decay, these are the decomposed fitting method based

Table 4: Result of fitting $M = (1.96161, 2.88108, -0.237176)$ by all the considered fitting algorithms

| | | | result | |
|---|---|---|---|---|
| method | abbr. | distance | $\mu_1$ | $(n_2, n_3, \gamma)$ |
| global optimization | (nm) | 0.7750 | | $(2.00498, 3.0149, -0.999348)$ |
| ordered moment adjusting method | (ma) | 0.0178 | | $(1.96161, 2.89884, -0.237176)$ |
| decomposed fitting of $\gamma$ | (eg) | 0.0067 | | $(1.95541, 2.88361, -0.237174)$ |
| decomposed fitting of $\rho_9$ | (r9) | 0.7731 | | $(2.00024, 3.00072, -0.999963)$ |
| decomposed fitting of $\rho_{99}$ | (r99) | 0.7686 | | $(1.99999, 2.99997, -0.995528)$ |
| decomposed fitting of $\lambda_d$ | (ed) | 0.7213 | | $(1.95541, 2.88361, 0.484102)$ |
| joint density based | (lh) | 0.6723 | 0.566744 | $(2.0254, 3.04949, 0.410575)$ |
| dominant eigenvalue of (lh) | (ld) | 0.7198 | 0.569103 | $(2.032, 3.06588, 0.454837)$ |

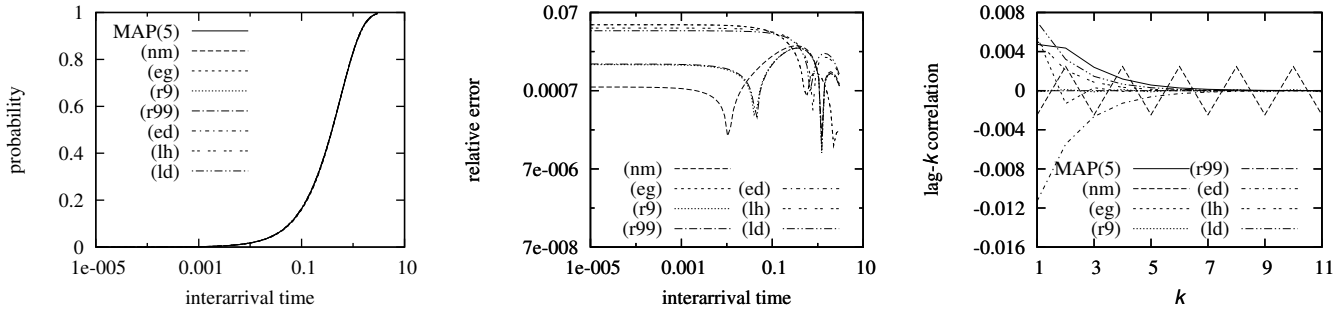


(a) The comparison of the CDFs (b) The error of the CDF fittings (c) The comparison of the correlation fitting

Figure 3: The comparison of cumulative distribution functions of the PH marginals and the correlation functions of the processes

higher correlation fittings, i.e., (r9) and (r99), and the Nelder-Mead method based global optimization (nm). The decomposed fitting method based $\gamma$ fitting (eg) fits the first lag correlation well since it is closely related to $\rho_1$ but all the other correlation coefficients are fitted badly. The reason is that this MAP(5) does not have geometrically decaying correlation structure. In case of (ed) the dominant eigenvalue is matched, but if $n_2 < 2$, which is the case now, the calculation of the correlation coefficient contains a minus sign, see (6), thus the lag-$k$ curve is reflected to the $x$-axis.

Figure 3(c) together with Figure 5(c) points out that the MAP(2) set has geometrically decaying correlation function, as given in (6), i.e., it is only possible to capture a geometric correlation structure.

**Queueing behavior** The queue length distributions generated by MAP arrivals are observed in an infinite buffer system with deterministic service time (MAP/D/1 queueing system) for two utilization levels, $\rho = 0.3$ and $\rho = 0.7$, in Figure 4. The utilization of the system is set through $D$, the deterministic service time, as $\rho = \frac{D}{\mu_1}$.

The queueing behavior of the MAP(5) and the fitted MAP(2)s with utilization level $\rho = 0.3$ are depicted in Figure 4(a) and all the MAP(2)s fit the original well.

Table 5: The mean queue lengths of the different scenarios

| | $\rho$ | |
|---|---|---|
| | 0.3 | 0.7 |
| MAP(5) | 0.365512305 | 1.524539289 |
| (nm) | 0.364296716 | 1.518172962 |
| (eg) | 0.362108709 | 1.488329671 |
| (r9) | 0.364158514 | 1.516371585 |
| (r99) | 0.364150473 | 1.51627773 |
| (ed) | 0.361219149 | 1.45877668 |
| (lh) | 0.367979806 | 1.558582197 |
| (ld) | 0.368298067 | 1.57042874 |

For $\rho = 0.7$, depicted in Figure 4(b), all the fitting procedures fit the original queue length distribution well. Table 6.1 summarizes the mean queue length for all the original and the fitted MAPs in case of both utilization levels.

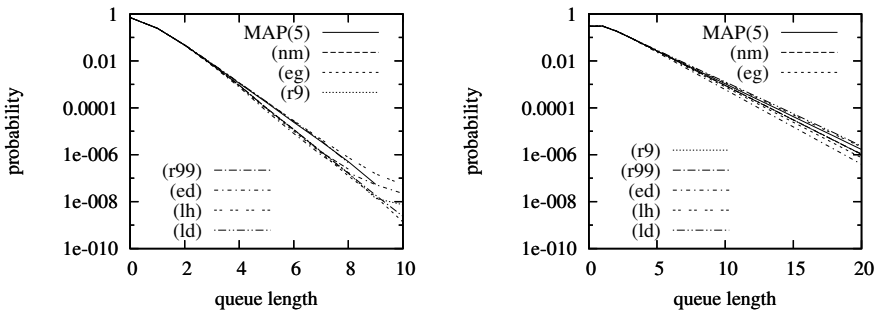


(a) $\rho = 0.3$ (b) $\rho = 0.7$

Figure 4: The queueing behavior of the MAPs

## 6.2 Matching inside the MAP(2) moments region

The MAP(3) with matrix representation

$$\mathbf{D}_0 = \begin{pmatrix} -0.1198 & 0.0008 & 0.0002 \\ 0 & -0.7509 & 0.0022 \\ 0 & 0 & -1.8641 \end{pmatrix},$$
$$\mathbf{D}_1 = \begin{pmatrix} 0,0915 & 0.025 & 0.0023 \\ 0.0022 & 0.6589 & 0.0876 \\ 1.71 \times 10^{-5} & 0.2432 & 1.6209 \end{pmatrix} \quad (29)$$

has moments inside the MAP(2) moments region: $(n_2 = 3.00618, n_3 = 10.0002, \gamma = 0.773409)$. The first raw moment is $\mu_1 = 0.999279$.

For further investigation the matrix representation of the fitted MAP(2)s are

$$\mathbf{D}_0^{(\mathrm{eg})} = \begin{pmatrix} -0.1648 & 0.0368 \\ 0 & -1.1109 \end{pmatrix} \quad \mathbf{D}_1^{(\mathrm{eg})} = \begin{pmatrix} 0.128 & 0 \\ 0.0046 & 1.1063 \end{pmatrix} \quad (30)$$

$$\mathbf{D}_0^{(\mathrm{lh})} = \begin{pmatrix} -0.7455 & 0.109 \\ 0 & -1.8626 \end{pmatrix} \quad \mathbf{D}_1^{(\mathrm{lh})} = \begin{pmatrix} 0.6365 & 0 \\ 0.22 & 1.6426 \end{pmatrix} \quad (31)$$

$$\mathbf{D}_0^{(\mathrm{ld})} = \begin{pmatrix} -0.7486 & 0.11 \\ 0 & -1.8634 \end{pmatrix} \quad \mathbf{D}_1^{(\mathrm{ld})} = \begin{pmatrix} 0.6386 & 0 \\ 0.221 & 1.6425 \end{pmatrix}. \quad (32)$$

Using the matrix representations in (29) and in (30) through (32) we can determine the important parameters of the MAPs. The CDF is plotted in Figure 5(a) and the relative errors of the CDF in Figure 5(b).

Based on the relative error diagram we could say that the MAP reduction performs better as expected.

Once more the lag correlation structure is investigated, as given in Figure 5(c) where two important things can be concluded. The moment based decomposed fitting method matches the correlation structure in this case, i.e., the input MAP(3) has geometric decaying correlation structure. The two MAP reductions give exactly the same result which means that the tail fitting in Section 5.2 is capable of performing similarly as the joint density function based fitting method. And another important conclusion of Figures 5(a), 5(b) and 5(c) is that even if the lag correlation structure is not captured that accurately the marginal distribution can be captured well. This shows the independence of the marginal distribution and the correlation structure in practice.

Table 6: The mean queue lengths of the different scenarios

| | $\rho$ | |
|---|---|---|
| | 0.3 | 0.7 |
| MAP(3) | 0.400511251 | 2.69909765 |
| (eg) | 0.373380958 | 1.851639028 |
| (lh) | 0.393725813 | 2.433117353 |
| (ld) | 0.393397716 | 2.421863393 |

Finally, we observed the queueing behavior of the processes in the same MAP/D/1 system as in the previous section with utilization levels $\rho = 0.3$ and $\rho = 0.7$ depicted in Figures 6(a) and 6(b), respectively. The mean queue lengths of the original, the matching and the joint density based fittings are summarized in Table 6.2. The "relatively bad" results of the moment distance based fitting/matching confirms that the Euclidean (or any equivalent) measure minimization based moment fitting/matching technique cannot capture all the important properties of a process in any arbitrary case.

In this experiment the decomposed fitting method could not fit the queue length distribution neither in case of lower nor in case of higher utilization levels.

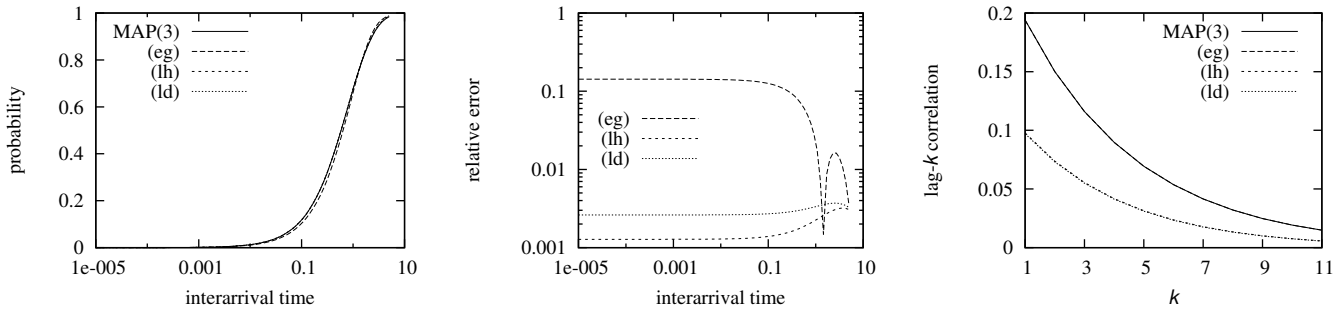


(a) The comparison of the CDFs (b) The error of the CDF fittings (c) The comparison of the correlation fitting

Figure 5: The comparison of cumulative distribution functions of the PH marginals and the correlation structure of the processes

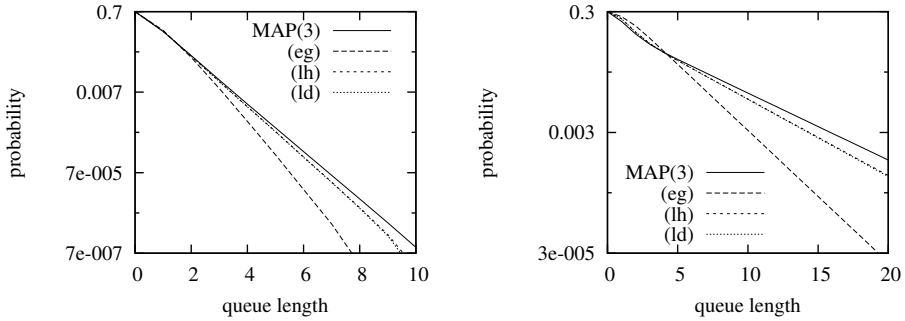


(a) $\rho = 0.3$ (b) $\rho = 0.7$

Figure 6: The queueing behavior of the MAPs

This confirms the previous conclusions that the practically exact fitting of the lag correlation structure does not ensure a better fit of the queue length distribution in this scenario.

# 7 Conclusion

We proposed to add two technical details to the existing MAP fitting methodology. The first one is to improve the efficiency of moments distance optimization procedures with a decomposition to nice components of the MAP bounding surface. The other proposal is to compute the distance of joint distribution functions of MAPs by efficiently computable matrix expressions.

We developed fitting procedures based on these proposals and evaluated their properties. Our experiences verified the expected advantages. The decomposed numerical fitting method reduces the numerical instability of the global optimization procedures applied for the whole boundary and the density function based distance measure resulted in an numerically efficient well behaving approximation.

During this paper we utilized the special results available currently only for the MAP(2) class. The proposed procedures are directly applicable for higher order MAPs when the analytical description (canonical form, moment bounds) of those classes become known.

# References


[1] Andrea Bobbio, András Horváth, and Miklós Telek. Matching three moments with minimal acyclic phase type distributions. *Stochastic Models*, pages 303–326, 2005.

[2] Levente Bodrog, Armin Heindl, Gábor Horváth, and Miklós Telek. A Markovian canonical form of second-order matrix-exponential processes. *European Journal of Operational Research*, 190(2):459–477, 2008.

[3] Levente Bodrog, András Horváth, and Miklós Telek. Moment characterization of matrix exponential and Markovian arrival processes. *Annals of Operations Research*, 160(1):51–68, 2008.

[4] G. Casale, E. Z. Zhang, and E. Smirni. Trace data characterization and fitting for Markov modeling. *Performance Evaluation*, 67:61–79, 2010.

[5] Armin Heindl. Inverse characterization of hyperexponential MAP(2)s. In *Proceedings of the 11th ASMTA*, pages 183–189, Magdeburg, Germany, 2004.

[6] Armin Heindl, Gábor Horváth, and Karsten Gross. Explicit inverse characterizations of acyclic MAPs of second order. In András Horváth and Miklós Telek, editors, *Formal Methods and Stochastic Models for Performance Evaluation*, pages 108–122, Budapest, Hungary, June 2006.

[7] Armin Heindl, Ken Mitchell, and Appie van de Liefvoort. Correlation bounds for second-order MAPs with application to queueing network decomposition. *Performance Evaluation*, 63:553–577, 2006.

[8] András Horváth, Gábor Horváth, and Miklós Telek. A joint moments based analysis of networks of MAP/MAP/1 queues. In *QEST*, pages 125–134, St Malo, France, Sept. 2008. IEEE CS.

[9] András Horváth and Miklós Telek. Markovian modeling of real data traffic: Heuristic phase type and MAP fitting of heavy tailed and fractal like samples. In *Performance Evaluation of Complex Systems: Techniques and Tools*, pages 405–434, 2002.

[10] Scott Kirkpatrick, Charles D. Gelatt, and Mario P. Vecchi. Optimization by simulated annealing. *Science*, 220:671–680, May 1983.

[11] G. Latouche and V. Ramaswami. *Introduction to Matrix-Analytic Methods in Stochastic Modeling*. Series on statistics and applied probability. ASA-SIAM, 1999.

[12] John Ashworth Nelder and Roger Mead. A simplex method for function minimization. *The Computer Journal*, 6(4):308–313, 1965.

[13] Takayuki Osogami and Mor Harchol-Balter. Necessary and sufficient conditions for representing general distributions by Coxians. In *Proceedings of the 12th International Conference on Modelling Tools and Techniques for Computer and Communication System Performance Evaluation*, pages 182–199, September 2003.

[14] Rainer Storn and Kenneth Price. Differential evolution - a simple and efficient adaptive scheme for global optimization over continuous spaces. Technical report.

[15] Miklós Telek and Armin Heindl. Moment bounds for acyclic discrete and continuous phase-type distributions of second order. In *Proceedings of UK Performance Evaluation Workshop*, 2002.

[16] Vladimír Černý. A thermodynamical approach to the travelling salesman problem: An efficient simulation algorithm. *Journal of Optimization Theory and Applications*, 45(1):41–51, January 1985.